Supplement of Atmos. Chem. Phys., 18, 14417–14432, 2018
https://doi.org/10.5194/acp-18-14417-2018-supplement

Atmospheric Chemistry and Physics
Open Access
EGU

Supplement of

Low-level summertime isoprene observed at a forested mountaintop site in southern China: implications for strong regional atmospheric oxidative capacity

Daocheng Gong et al.

Correspondence to: Boguang Wang (tbongue@jnu.edu.cn)

Text S1. Estimation of regional mixing ratios of daytime OH

It is well known that BTEX (benzene, toluene, ethylbenzene, and m,p-xylene) are the most important aromatic hydrocarbons regarding their universal anthropogenic sources. Because of their atmospheric lifetimes of up to several days (Table S1), BTEX can undergo long-range transport. The ratio of two aromatics that share common emission sources but with different reactivities with hydroxyl radical (OH) can be used as a measure of photochemical oxidation by OH (Parrish et al., 2007;Shiu et al., 2007). Thus, BTEX provide particularly promising capabilities for following photochemical processing on timescales of hours to days. In this study, we chose three pairs of aromatic species: toluene/benzene, ethylbenzene/benzene, and *m*,*p*-xylene/benzene.

During daytime, decreasing of BTEX levels along transport path owes mainly to atmospheric dilution and reaction with OH. The chemical removal of BTEX by OH can be expressed as followings:

$Benzene + OH \rightarrow$ products $\quad k_{benzene,OH} = 2.3 \times 10^{-12}\, e^{-190/T}$ (R1)

$Toluene + OH \rightarrow$ products $\quad k_{Toluene,OH} = 1.8 \times 10^{-12}\, e^{340/T}$ (R2)

$Ethylbenzene + OH \rightarrow$ products $\quad k_{Ethylbenzene,OH} = 7.0 \times 10^{-12}$ (R3)

$m,p - Xylene + OH \rightarrow$ products $\quad k_{m,p-Xylene,OH} = 1.89 \times 10^{-11}$ (R4)

Thus, mixing ratios of BTEX at the sampling time can be expressed as follows, for example, in the case of benzene,

$$[B]_t = [B]_0 \times e^{-[OH]\times k_{B,OH}\times t} \times f_{d,B} \quad \text{(Eq.1)}$$

where $[B]_0$ and $[B]_t$ represents the mixing ratios of measured benzene at the start and after transport time t that air mass spent in the atmosphere, respectively. $k_{B,OH}$ represents the temperature dependent reaction rate coefficient of benzene with OH, which was taken from the IUPAC database (http://iupac.pole-ether.fr/) (Atkinson et al., 2006). $[OH]$ represents the regional concentrations of OH. $f_{d,B}$ represents the dilution factor of benzene in the atmosphere.

Toluene, ethylbenzene and m,p-xylene react faster with OH than benzene. In this study, we assuming the rates of turbulent mixing and horizontal convection are similar for BTEX. Therefore, during the transport time Δt, the dilution factor of BTEX are the same. Then rearranging Eq.1 and extending this analysis to BTEX will yield the following equations.

$$[OH]_{T/B} = \frac{1}{t\times(k_{T,OH}-k_{B,OH})} \times \left[\ln\left(\frac{[T]}{[B]}\right)_0 - \ln\left(\frac{[T]}{[B]}\right)_t\right] \quad \text{(Eq.2)}$$

$$[OH]_{E/B} = \frac{1}{t \times (k_{E,OH} - k_{B,OH})} \times \left[\ln\left(\frac{[E]}{[B]}\right)_0 - \ln\left(\frac{[E]}{[B]}\right)_t \right] \quad \text{(Eq.3)}$$

$$[OH]_{X/B} = \frac{1}{t \times (k_{X,OH} - k_{B,OH})} \times \left[\ln\left(\frac{[X]}{[B]}\right)_0 - \ln\left(\frac{[X]}{[B]}\right)_t \right] \quad \text{(Eq.4)}$$

Where $[OH]_{T/B}$, $[OH]_{E/B}$, and $[OH]_{X/B}$ represent the estimated regional mixing ratios of OH by three aromatic ratios. It should be noted that the data included only daytime observations between 09:00–15:00 LST when the aromatic ratios presented a smoothly decreasing trend (Fig. S3). In addition, the X/B ratio may not work well in comparison with T/B and E/B owing to the relatively short lifetime of *m,p*-xylene (Table S1). Indeed, results derived from X/B are significantly lower than those from T/B and E/B, and we use the mean values derived by T/B and E/B in this study. The scatterplots of the regional mixing ratios of OH derived from the three ratios were presented in the Fig. S8, and the diurnal patterns were presented in the Fig. S9.

Text S2. Calculation of initial isoprene

The first-stage oxidation of isoprene (ISO), MVK and MACR by reaction with OH during the day, and with NO_3 at night, can be described by the following reactions:

$ISO + OH \rightarrow y_{MACR,OH}\, MACR + y_{MVK,OH}\, MVK$	$k_{ISO,OH} = 2.7 \times 10^{-11}\, e^{390/T}$	(R5)
$MVK + OH \rightarrow products$	$k_{MVK,OH} = 2.6 \times 10^{-12}\, e^{610/T}$	(R6)
$MACR + OH \rightarrow$ products	$k_{MACR,OH} = 8.0 \times 10^{-12}\, e^{380/T}$	(R7)
$ISO + NO_3 \rightarrow y_{MACR,NO_3}\, MACR + y_{MVK,NO_3}\, MVK$	$k_{ISO,NO_3} = 2.95 \times 10^{-12}\, e^{-450/T}$	(R8)
$MVK + NO_3 \rightarrow$ products	$k_{MVK,NO_3} < 6.0 \times 10^{-16}$	(R9)
$MACR + NO_3 \rightarrow$ products	$k_{MACR,NO_3} = 3.4 \times 10^{-15}$	(R10)

Where k is the temperature dependent reaction rate coefficients taken from the IUPAC database (http://iupac.pole-ether.fr/) (Atkinson et al., 2006). y are yields of MVK and MACR from isoprene reaction with OH and NO_3. T is the temperature (unit in K).

Then, the product/parent ratios, *i.e.* [MVK]/[ISO] and [MVK]/[ISO], can be calculated as a function of the rate constants (k), yield (y), reaction time (Δt) and radical concentration ([OH] and [NO_3]):

$$\left(\frac{[MVK]}{[ISO]}\right)_D = \frac{y_{MVK,OH}\, k_{ISO,OH}}{(k_{MVK,OH} - k_{ISO,OH})} \times \left[1 - e^{(k_{ISO,OH} - k_{MVK,OH})\,[OH]\,\Delta t}\right] \quad \text{(Eq.5)}$$

$$\left(\frac{[MACR]}{[ISO]}\right)_D = \frac{y_{MACR,OH}\, k_{ISO,OH}}{(k_{MACR,OH} - k_{ISO,OH})} \times \left[1 - e^{(k_{ISO,OH} - k_{MACR,OH})\,[OH]\,\Delta t}\right] \quad \text{(Eq.6)}$$

$$\left(\frac{[MVK]}{[ISO]}\right)_N = \frac{y_{MVK,NO_3}\, k_{ISO,NO_3}}{(k_{MVK,NO_3} - k_{ISO,NO_3})} \times \left[1 - e^{(k_{ISO,NO_3} - k_{MVK,NO_3})\,[NO_3]\,\Delta t}\right] \quad \text{(Eq.7)}$$

$$\left(\frac{[MACR]}{[ISO]}\right)_N = \frac{y_{MACR,NO_3}\, k_{ISO,NO_3}}{(k_{MACR,NO_3} - k_{ISO,NO_3})} \times \left[1 - e^{(k_{ISO,NO_3} - k_{MACR,NO_3})\,[NO_3]\,\Delta t}\right] \quad \text{(Eq.8)}$$

Where [*ISO*], [*MVK*] and [*MACR*] represent the observed isoprene, MVK and MACR. [*OH*] and [NO_3] represent daytime OH and nighttime NO_3, respectively. *D* and *N* represent daytime and nighttime periods, respectively. Δt is the atmospheric reaction time of isoprene, representing the time of isoprene in the atmosphere between emission and detection.

Initial isoprene $[ISO]_i$, the total isoprene emissions that have been released into the sample air masses, can be effectively calculated via reverse integration of isoprene's first-stage oxidation:

$$[ISO]_{i,D} = [ISO] \times e^{(k \times [OH] \times \Delta t)} \quad \text{(Eq.9)}$$

$$[ISO]_{i,N} = [ISO] \times e^{(k \times [NO_3] \times \Delta t)} \quad \text{(Eq.10)}$$

By determining the concentration of radical (*i.e.* OH and NO_3) and atmospheric reaction time of isoprene, the initial isoprene can be calculated.

Two issues arise when applying this "back-of-the-envelope" method to the present study (Wolfe et al., 2016). First, the yields from OH-initiated isoprene oxidation are a nonlinear function of nitrogen oxide (NO). Previous applications of this method (de Gouw, 2005;Roberts et al., 2006;Stroud et al., 2001;Karl et al., 2007;Kuhn et al., 2007) have assumed lab-derived high-NO yields of 0.33 and 0.23 for MVK and MACR, respectively (Atkinson and Arey, 2003a), but this may not be appropriate in the present study. Thus we chose the yields derived from the latest Master Chemical Mechanism (MCM) v3.3.1 (Jenkin et al., 2015). The resulting yield curves are interpolated to observed NO mixing ratios (Fig. S7). The yields from NO_3-initiated isoprene oxidation are constants (Table S1). Second, the implied initial isoprene is depended on the mixing ratios of radical and the atmospheric reaction time of isoprene. Thus in this study we introduce the term "exposure" (de Gouw, 2005;Jimenez et al., 2009;Wolfe et al., 2016) defined here as the product of radical concentration and reaction time ($Exposure = [Radical] \times \Delta t$). Exposures can be obtained by the following two-step process.

First, for any given exposure, a daughter/parent ratio can be expected based on Eq. (5–8), and the theoretical line of [MVK]/[isoprene] versus [MACR]/[isoprene] can be depicted (Stroud et al., 2001;Apel et al., 2002;Roberts et al., 2006;Guo et al., 2012;Wolfe et al., 2016). The range of exposure thus can be derived by comparing the expected daughter/parent ratio with observed data. Then the range of the ratio of initial over observed isoprene (ISO_i/ISO_o) can be calculated based on Eq. (9–10). Fig. S10 compares the relationship of measured data against theoretical trends predicted by the sequential reaction calculation for the daytime and nighttime hours. It can be seen that the observed [MVK]/[isoprene] versus [MACR]/[isoprene] exhibit a tight linear correlation (R^2=0.68 and 0.72 for daytime and nighttime periods, respectively). The measured data fit the predicted line well, although most of the measured data are above the predicted line, which is consistent with some previous studies (Stroud et al., 2001;Apel et al., 2002;Guo et al., 2012). Apart from the uncertainties mentioned in the Section 2.5 of the manuscript, the additional

sources of MVK and MACR from isoprene oxidation by daytime NO_3 (Xue et al., 2016) and nighttime OH (Lu et al., 2014) which both were not taken into account in the present study might also be the causes. The theoretical slope agrees well with observations, indicating OH exposures of 0.1–12 × 10^6 molecules cm^{-3} h and NO_3 exposures of 4–28 × 10^8 molecules cm^{-3} h for daytime and nighttime periods, respectively.

Second, detailed profiles of exposure can be directly calculated from the observed daughter/parent ratios by inverting Eq. (5–8):

$$EXPO_{OH,MVK} = \frac{\ln\left(1-\frac{[MVK]}{[ISO]}\times\frac{k_{MVK,OH}-k_{ISO,OH}}{y_{MVK,OH}\,k_{ISO,OH}}\right)}{\left(k_{ISO,OH}-k_{MVK,OH}\right)} \quad \text{(Eq.11)}$$

$$EXPO_{OH,MACR} = \frac{\ln\left(1-\frac{[MACR]}{[ISO]}\times\frac{k_{MACR,OH}-k_{ISO,OH}}{y_{MACR,OH}\,k_{ISO,OH}}\right)}{\left(k_{ISO,OH}-k_{MACR,OH}\right)} \quad \text{(Eq.12)}$$

$$EXPO_{NO_3,MVK} = \frac{\ln\left(1-\frac{[MVK]}{[ISO]}\times\frac{k_{MVK,NO_3}-k_{ISO,NO_3}}{y_{MVK,NO_3}\,k_{ISO,NO_3}}\right)}{\left(k_{ISO,NO_3}-k_{MVK,NO_3}\right)} \quad \text{(Eq.13)}$$

$$EXPO_{NO_3,MACR} = \frac{\ln\left(1-\frac{[MACR]}{[ISO]}\times\frac{k_{MACR,NO_3}-k_{ISO,NO_3}}{y_{MACR,NO_3}\,k_{ISO,NO_3}}\right)}{\left(k_{ISO,NO_3}-k_{MACR,NO_3}\right)} \quad \text{(Eq.14)}$$

Where $EXPO_{OH,\,MVK}$, $EXPO_{OH,\,MACR}$, $EXPO_{NO_3,\,MVK}$, and $EXPO_{NO_3,\,MACR}$ represent the derived exposures from [MVK]/[isoprene] and [MACR]/[isoprene] for daytime and nighttime periods.

Calculated daytime OH exposures and nighttime NO_3 exposures range from 1.0 × 10^5 to 1.3 × 10^7 molecules cm^{-3} h and 3.5× 10^8 to 3.2 × 10^9 molecules cm^{-3} h, respectively (Fig. S11). The OH and NO_3 exposures derived from two ratios exhibit a good linear correlation (R^2=0.63 and 0.70 for OH and NO_3, respectively), and results derived from [MACR]/[isoprene] are 4% and 18% lower than those from [MVK]/[isoprene] on average, respectively, and we use the mean of these two values. The median and mean OH exposure is 1.9 and 2.5 × 10^6 molecules cm^{-3} h, respectively. For NO_3 exposure, the median and mean value is close (15.8 and 16.2 × 10^8 molecules cm^{-3} h, respectively).

Text S3. Data processing, graph plotting and graphical source identification by R

In this study, the open source R package "openair" was utilized for data processing and graph plotting (Carslaw and Ropkins, 2012;Carslaw, 2015). Specifically, for those dedicated functions used, the "transform", "selectByDate", "merge" and "subset" functions were used to calculate and filter the data. The "quantile", "summary" and "t.test" functions were used to do statistical analysis. The "timePlot" function was used to plot time series of measured species. The "plot" function was used to plot scatter and diagram diurnal variations. In particular, the "polarPlot" function was used for source identification.

The lifetimes of MVK and MACR by OH loss is 1.9 and 1.0 hours, respectively, assuming 12-h daytime OH = 8.0 × 10^6 molecules cm^{-3} (Table S1). The average daytime wind speed was 3.9 ± 0.2 m s^{-1} at the site,

and the distance between the sampling sit and the nearest urban center is 38 km (Fig. S12), the air parcel from upwind locations would spend about 2.7 hours to arrive at the sampling site. This is enough time for the depletion of MVK and MACR along the traveling path during the daytime. However, the nighttime chemical oxidation of MVK and MACR was slow, with lifetimes of MVK and MACR by NO_3 oxidation of 0.5 years and 72 hours, respectively, assuming 12-h nighttime $NO_3 = 5.0 \times 10^8$ molecules cm^{-3} (Table S1). Apart from biogenic sources, the anthropogenic sources of MVK and MACR, *e.g.* motor vehicles, biomass burning and industrial sources, have been reported by some previous studies (Borbon et al., 2001;Wagner and Kuttler, 2014;Hsieh et al., 2017;Diao et al., 2016). Therefore, the regional transport of MVK- or MACR- laden air could affect the observed nighttime (MVK+MACR)/isoprene ratios at the site.

Hence, the "polarPlot" technique was used for source identification in this study. In "polarPlot" drawing, the species concentrations are shown to vary by wind speed and wind direction, and plots are shown as a continuous surface, and the surfaces are calculated through modeling using smoothing techniques. These plots have been proved to be useful for the quick gaining of a graphical impression of potential sources' influences at a location in recent publications that describe or use the technique (Valach et al., 2014;Chang et al., 2017). Fig. S13 shows the polarplots of isoprene, MVK and MACR during the study. During the sampling periods, the air masses reaching the site were mainly from the southwest and northeast directions. The red dotted sectorial domains are interpreted as the regional transport interference as the concentrations of species increase with increasing wind speed. The high levels of species at high wind speeds most likely came from the nearby urban centers. Therefore, measurements that are deemed to be affected by regional transport are all excluded from the dataset in the analysis.

References

Apel, E. C., Riemer, D. D., Hills, A., Baugh, W., Orlando, J., Faloona, I., Tan, D., Brune, W., Lamb, B., Westberg, H., Carroll, M. A., Thornberry, T., and Geron, C. D.: Measurement and interpretation of isoprene fluxes and isoprene, methacrolein, and methyl vinyl ketone mixing ratios at the PROPHET site during the 1998 Intensive, Journal of Geophysical Research-Atmospheres, 107, 15, 10.1029/2000jd000225, 2002.

Atkinson, R., and Arey, J.: Gas-phase tropospheric chemistry of biogenic volatile organic compounds: a review, Atmos Environ, 37, S197-S219, 10.1016/S1352-2310(03)00391-1, 2003a.

Atkinson, R., and Arey, J.: Atmospheric degradation of volatile organic compounds, Chem Rev, 103, 4605-4638, 10.1021/cr0206420, 2003b.

Atkinson, R., Baulch, D. L., Cox, R. A., Crowley, J. N., Hampson, R. F., Hynes, R. G., Jenkin, M. E., Rossi, M. J., and Troe, J.: Evaluated kinetic and photochemical data for atmospheric chemistry: Volume II – gas phase reactions of organic species, Atmos Chem Phys, 6, 3625-4055, 10.5194/acp-6-3625-2006, 2006.

Borbon, A., Fontaine, H., Veillerot, M., Locoge, N., Galloo, J. C., and Guillermo, R.: An investigation into the traffic-related fraction of isoprene at an urban location, Atmos Environ, 35, 3749-3760, 10.1016/S1352-2310(01)00170-4, 2001.
Carslaw, D. C., and Ropkins, K.: openair — An R package for air quality data analysis, Environmental Modelling & Software, 27-28, 52-61, 10.1016/j.envsoft.2011.09.008, 2012.
Chang, Y., Huang, K., Deng, C., Zou, Z., Liu, S., and Zhang, Y.: First long-term and near real-time measurement of atmospheric trace elements in Shanghai, China, Atmospheric Chemistry and Physics Discussions, 1-49, 10.5194/acp-2017-613, 2017.
de Gouw, J. A.: Budget of organic carbon in a polluted atmosphere: Results from the New England Air Quality Study in 2002, Journal of Geophysical Research, 110, 22, 10.1029/2004jd005623, 2005.
Diao, L. J., Choi, Y., Czader, B., Li, X. S., Pan, S., Roy, A., Souri, A. H., Estes, M., and Jeon, W.: Discrepancies between modeled and observed nocturnal isoprene in an urban environment and the possible causes: A case study in Houston, Atmos Res, 181, 257-264, 10.1016/j.atmosres.2016.07.009, 2016.
Guo, H., Ling, Z. H., Simpson, I. J., Blake, D. R., and Wang, D. W.: Observations of isoprene, methacrolein (MAC) and methyl vinyl ketone (MVK) at a mountain site in Hong Kong, Journal of Geophysical Research-Atmospheres, 117, 13, 10.1029/2012jd017750, 2012.
Hsieh, H.-C., Ou-Yang, C.-F., and Wang, J.-L.: Revelation of Coupling Biogenic with Anthropogenic Isoprene by Highly Time-Resolved Observations, Aerosol and Air Quality Research, 17, 721-729, 10.4209/aaqr.2016.04.0133, 2017.
Jenkin, M. E., Young, J. C., and Rickard, A. R.: The MCM v3.3.1 degradation scheme for isoprene, Atmos Chem Phys, 15, 11433-11459, 10.5194/acp-15-11433-2015, 2015.
Jimenez, J. L., Canagaratna, M. R., Donahue, N. M., Prevot, A. S., Zhang, Q., Kroll, J. H., DeCarlo, P. F., Allan, J. D., Coe, H., Ng, N. L., Aiken, A. C., Docherty, K. S., Ulbrich, I. M., Grieshop, A. P., Robinson, A. L., Duplissy, J., Smith, J. D., Wilson, K. R., Lanz, V. A., Hueglin, C., Sun, Y. L., Tian, J., Laaksonen, A., Raatikainen, T., Rautiainen, J., Vaattovaara, P., Ehn, M., Kulmala, M., Tomlinson, J. M., Collins, D. R., Cubison, M. J., Dunlea, E. J., Huffman, J. A., Onasch, T. B., Alfarra, M. R., Williams, P. I., Bower, K., Kondo, Y., Schneider, J., Drewnick, F., Borrmann, S., Weimer, S., Demerjian, K., Salcedo, D., Cottrell, L., Griffin, R., Takami, A., Miyoshi, T., Hatakeyama, S., Shimono, A., Sun, J. Y., Zhang, Y. M., Dzepina, K., Kimmel, J. R., Sueper, D., Jayne, J. T., Herndon, S. C., Trimborn, A. M., Williams, L. R., Wood, E. C., Middlebrook, A. M., Kolb, C. E., Baltensperger, U., and Worsnop, D. R.: Evolution of organic aerosols in the atmosphere, Science, 326, 1525-1529, 10.1126/science.1180353, 2009.
Karl, T., Guenther, A., Yokelson, R. J., Greenberg, J., Potosnak, M., Blake, D. R., and Artaxo, P.: The tropical forest and fire emissions experiment: Emission, chemistry, and transport of biogenic volatile organic compounds in the lower atmosphere over Amazonia, Journal of Geophysical Research-Atmospheres, 112, 17, 10.1029/2007jd008539, 2007.
Kuhn, U., Andreae, M. O., Ammann, C., Araujo, A. C., Brancaleoni, E., Ciccioli, P., Dindorf, T., Frattoni, M., Gatti, L. V., Ganzeveld, L., Kruijt, B., Lelieveld, J., Lloyd, J., Meixner, F. X., Nobre, A. D., Poschl, U., Spirig, C., Stefani, P., Thielmann, A., Valentini, R., and Kesselmeier, J.: Isoprene and monoterpene fluxes from Central Amazonian rainforest inferred from tower-based and airborne measurements, and implications on the atmospheric chemistry and the local carbon budget, Atmos Chem Phys, 7, 2855-2879, 10.5194/acp-7-2855-2007, 2007.
Lu, K. D., Rohrer, F., Holland, F., Fuchs, H., Brauers, T., Oebel, A., Dlugi, R., Hu, M., Li, X., Lou, S. R., Shao, M., Zhu, T., Wahner, A., Zhang, Y. H., and Hofzumahaus, A.: Nighttime observation and chemistry of HOx in the Pearl River Delta and Beijing in summer 2006, Atmos Chem Phys, 14, 4979-4999, 10.5194/acp-14-4979-2014, 2014.
Parrish, D. D., Stohl, A., Forster, C., Atlas, E. L., Blake, D. R., Goldan, P. D., Kuster, W. C., and de Gouw, J. A.: Effects of mixing on evolution of hydrocarbon ratios in the troposphere, Journal of Geophysical Research-Atmospheres, 112, 10.1029/2006jd007583, 2007.

Roberts, J. M., Marchewka, M., Bertman, S. B., Goldan, P., Kuster, W., de Gouw, J., Warneke, C., Williams, E., Lerner, B., Murphy, P., Apel, E., and Fehsenfeld, F. C.: Analysis of the isoprene chemistry observed during the New England Air Quality Study (NEAQS) 2002 intensive experiment, Journal of Geophysical Research-Atmospheres, 111, 10.1029/2006jd007570, 2006.
Shiu, C. J., Liu, S. C., Chang, C. C., Chen, J. P., Chou, C. C. K., Lin, C. Y., and Young, C. Y.: Photochemical production of ozone and control strategy for Southern Taiwan, Atmos Environ, 41, 9324-9340, 10.1016/j.atmosenv.2007.09.014, 2007.
Stroud, C. A., Roberts, J. M., Goldan, P. D., Kuster, W. C., Murphy, P. C., Williams, E. J., Hereid, D., Parrish, D., Sueper, D., Trainer, M., Fehsenfeld, F. C., Apel, E. C., Riemer, D., Wert, B., Henry, B., Fried, A., Martinez-Harder, M., Harder, H., Brune, W. H., Li, G., Xie, H., and Young, V. L.: Isoprene and its oxidation products, methacrolein and methylvinyl ketone, at an urban forested site during the 1999 Southern Oxidants Study, Journal of Geophysical Research-Atmospheres, 106, 8035-8046, 10.1029/2000jd900628, 2001.
Valach, A. C., Langford, B., Nemitz, E., MacKenzie, A. R., and Hewitt, C. N.: Concentrations of selected volatile organic compounds at kerbside and background sites in central London, Atmos Environ, 95, 456-467, 10.1016/j.atmosenv.2014.06.052, 2014.
Wagner, P., and Kuttler, W.: Biogenic and anthropogenic isoprene in the near-surface urban atmosphere—a case study in Essen, Germany, The Science of the total environment, 475, 104-115, 10.1016/j.scitotenv.2013.12.026, 2014.
Wolfe, G. M., Kaiser, J., Hanisco, T. F., Keutsch, F. N., de Gouw, J. A., Gilman, J. B., Graus, M., Hatch, C. D., Holloway, J., Horowitz, L. W., Lee, B. H., Lerner, B. M., Lopez-Hilifiker, F., Mao, J., Marvin, M. R., Peischl, J., Pollack, I. B., Roberts, J. M., Ryerson, T. B., Thornton, J. A., Veres, P. R., and Warneke, C.: Formaldehyde production from isoprene oxidation across NOx regimes, Atmos Chem Phys, 16, 2597-2610, 10.5194/acp-16-2597-2016, 2016.
Xu, Z., Wang, T., Xue, L. K., Louie, P. K. K., Luk, C. W. Y., Gao, J., Wang, S. L., Chai, F. H., and Wang, W. X.: Evaluating the uncertainties of thermal catalytic conversion in measuring atmospheric nitrogen dioxide at four differently polluted sites in China, Atmos Environ, 76, 221-226, 10.1016/j.atmosenv.2012.09.043, 2013.
Xue, L. K., Gu, R. R., Wang, T., Wang, X. F., Saunders, S., Blake, D., Louie, P. K. K., Luk, C. W. Y., Simpson, I., Xu, Z., Wang, Z., Gao, Y., Lee, S. C., Mellouki, A., and Wang, W. X.: Oxidative capacity and radical chemistry in the polluted atmosphere of Hong Kong and Pearl River Delta region: analysis of a severe photochemical smog episode, Atmos Chem Phys, 16, 9891-9903, 10.5194/acp-16-9891-2016, 2016.
Zha, Q.: Measurement of nitrous acid (HONO) and the implications to photochemical pollution, MPhil dissertation, Department of Civil and Environmental Engineering, The Hong Kong Polytechnic University, 2015.

Tables

Table S1. Rate constants and lifetime for isoprene, MVK and MACR, and yields of MVK and MACR from the isoprene reactions.

Compound	Rate constants [a] with			Yield [b] from isoprene reaction with / (lifetime [b] due to)		
	OH	NO_3	O_3	OH	NO_3	O_3
Isoprene	1.0×10^{-10}	7.0×10^{-13}	1.3×10^{-17}	- / 0.4 h	- / 0.8 h	- / 24 h
MVK	2.0×10^{-11}	3.2×10^{-16}	5.2×10^{-18}	0.33 / 1.9 h	0.035 / 0.5 yr	0.16 / 61 h
MACR	2.9×10^{-11}	3.7×10^{-15}	1.2×10^{-18}	0.23 / 1.0 h	0.035 / 72 h	0.41 / 10 d
Benzene	1.2×10^{-12}	$<3.0\times10^{-17}$	$<1.0\times10^{-21}$	- / 9.5 d [c]	- / >4 yr	- / >4.5 yr
Toluene	5.6×10^{-12}	7.8×10^{-17}	$<1.0\times10^{-21}$	- / 2.1 d [c]	- / 1.8 yr	- / >4.5 yr
Ethylbenzene	7.0×10^{-12}	$<6.0\times10^{-16}$	$<1.0\times10^{-21}$	- / 1.7 d [c]	-	-
m,p-Xylene	1.9×10^{-11}	3.8×10^{-16}	$<1.0\times10^{-21}$	- / 0.6 d [c]	- / 0.5 yr	- / >5 yr

[a] The 298 K rate constants (unit in cm^3 $molecule^{-1}$ s^{-1}) are taken from Atkinson and Arey (2003b), Atkinson et al. (2006) and IUPAC database (http://iupac.pole-ether.fr/).

[b] (Atkinson and Arey, 2003a, b) and references therein. Lifetime calculated at 298 K using the following: for OH radical reactions, a 12-h daytime average of 8.0×10^6 molecules cm^{-3}; for NO_3 radical reactions, a 12-h nighttime average of 5.0×10^8 molecules cm^{-3}; and for O_3, a 24-h average of 1.0×10^{12} molecules cm^{-3}.

[c] For a 12-h daytime average OH radical concentration of 2.0×10^6 molecules cm^{-3}.

Figures

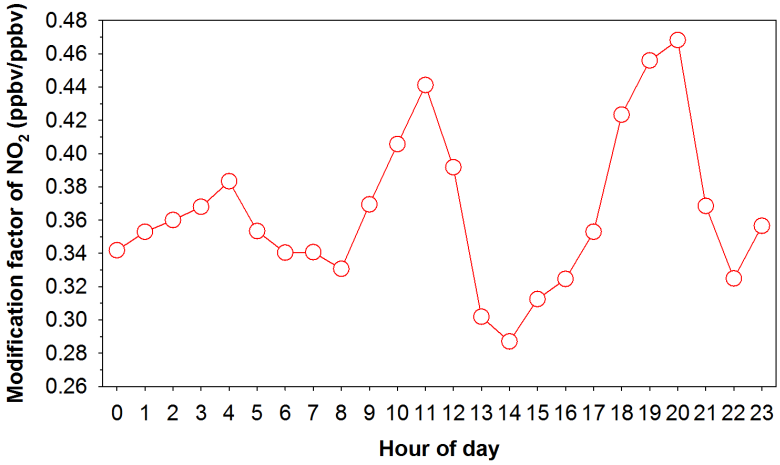

Fig. S1: Hourly modification factor of NO_2 during Jul 15 – Aug 17 2016 at the Nanling site. The data in the figure are reproduced from the study conducted at a high-altitude mountain site (Mt. Tai) in central-eastern China by Xu et al. (2013).

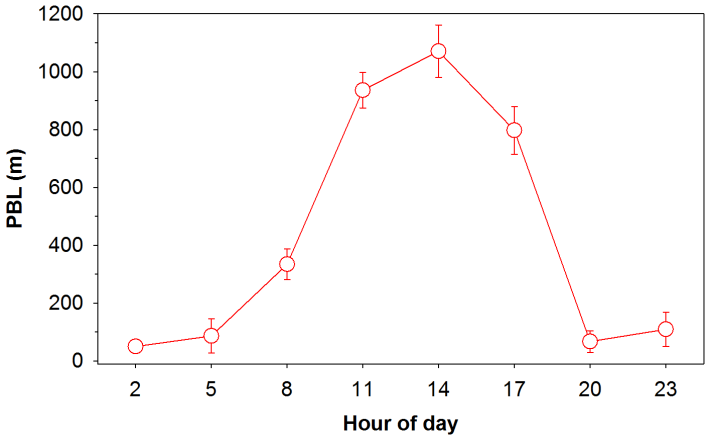

Fig. S2: Diurnal variation of the Planetary Boundary Layer (PBL) height (data provided by Real-time Environmental Applications and Display System, https://ready.arl.noaa.gov/READYamet.php, last accessed: 14 July 2018) at Nanling site (1,690 m a.s.l.) during Jul 15–Aug 17 2016. Error bars indicate the 95% confidence interval.

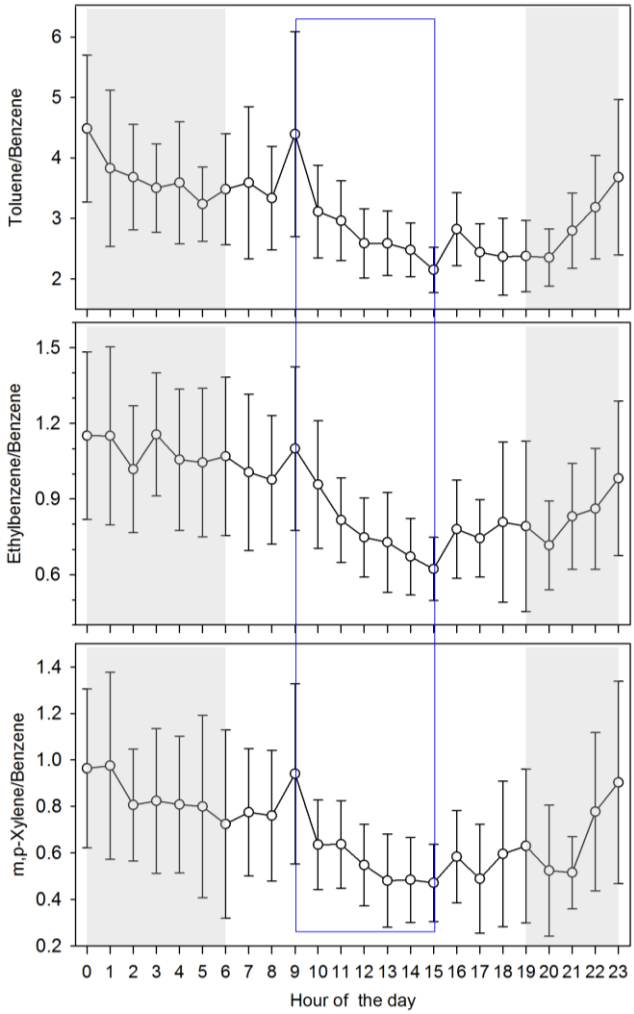

Fig. S3: Diurnal variations of toluene/benzene, ethylbenzene/benzene and m,p-xylene/benzene ratios at Nanling site during Jul 15–Aug 17 2016. Shaded regions denote the nighttime periods. Error bars indicate the 95% confidence interval. Blue boxed area denotes periods for the calculating of regional mixing ratios of daytime OH.

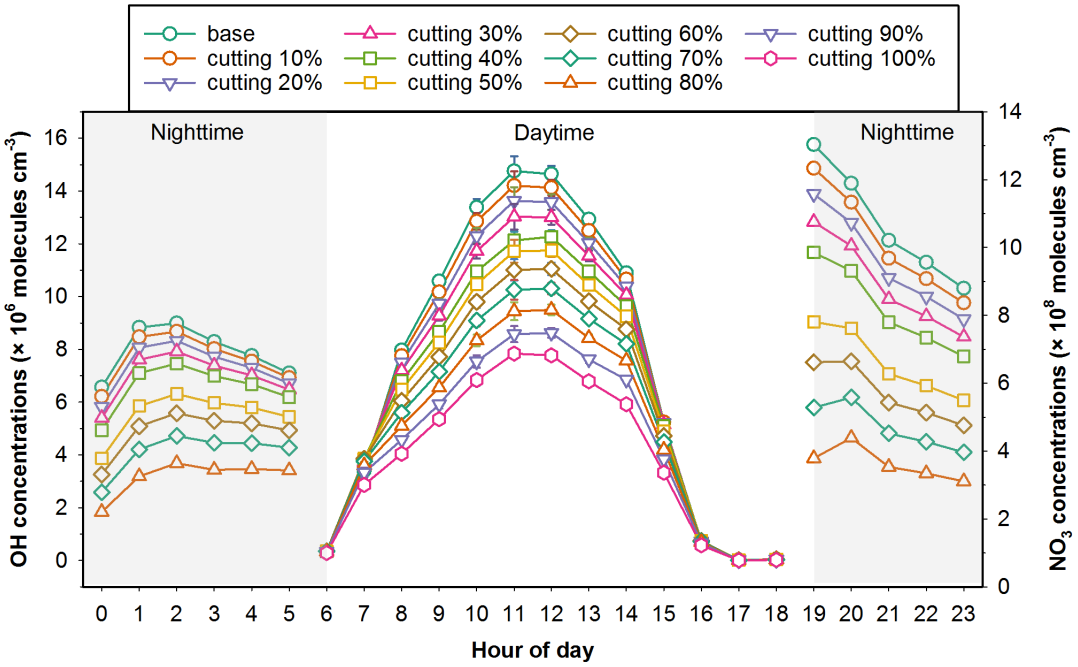

Fig. S4: Sensitivity analysis of PBM-MCM modelled daytime OH and nighttime NO_3 with reduced NO_2 concentrations for the period Aug 11 – Aug 15 2016.

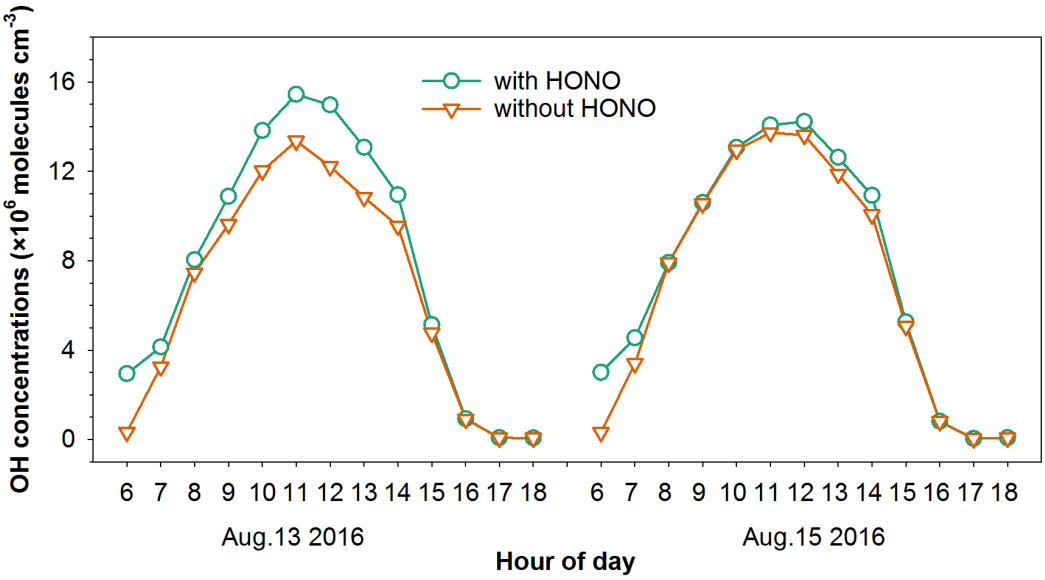

Fig. S5: Sensitivity analysis of PBM-MCM modelled daytime OH with and without HONO for the period Aug 13 and Aug 15 2016. The HONO data was obtained from the study conducted at a background site (Hok Tsui) in Hong Kong in autumn 2012 by Zha (2015).

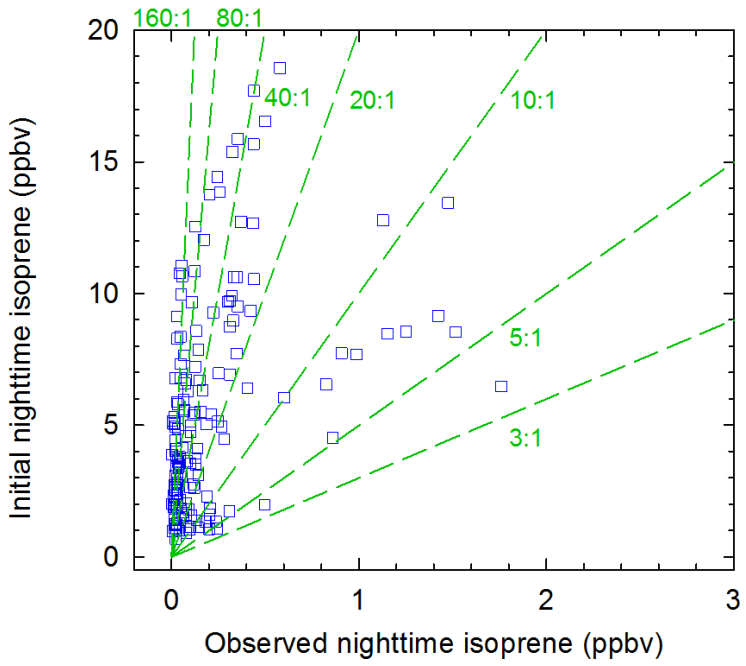

Fig. S6: Comparison of observed and initial isoprene mixing ratios at night. Green dashed lines denote slopes for different ratios of initial to observed isoprene.

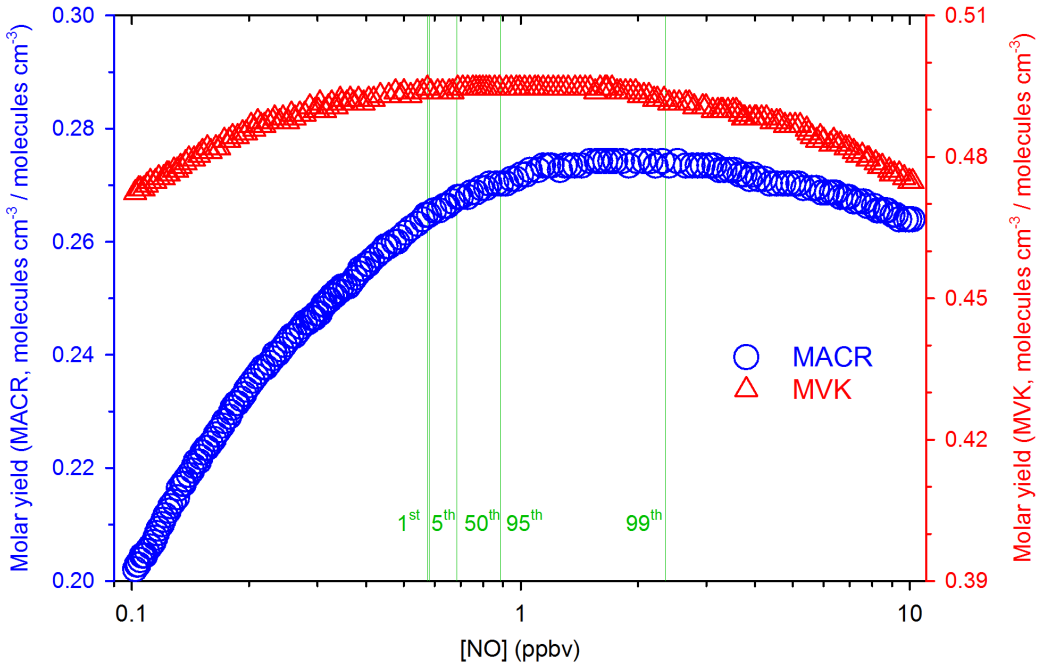

Fig. S7: Molar yields of the main first-generation products (MVK and MACR) of the OH-initiated oxidation of isoprene as a function of NO mixing ratio, at 298 K, as represented in MCM v3.3.1 (Jenkin et al., 2015). Thin green vertical lines denote, from left to right, the 1st, 5th, 50th, 95th and 99th percentiles of hourly NO observed during the present study.

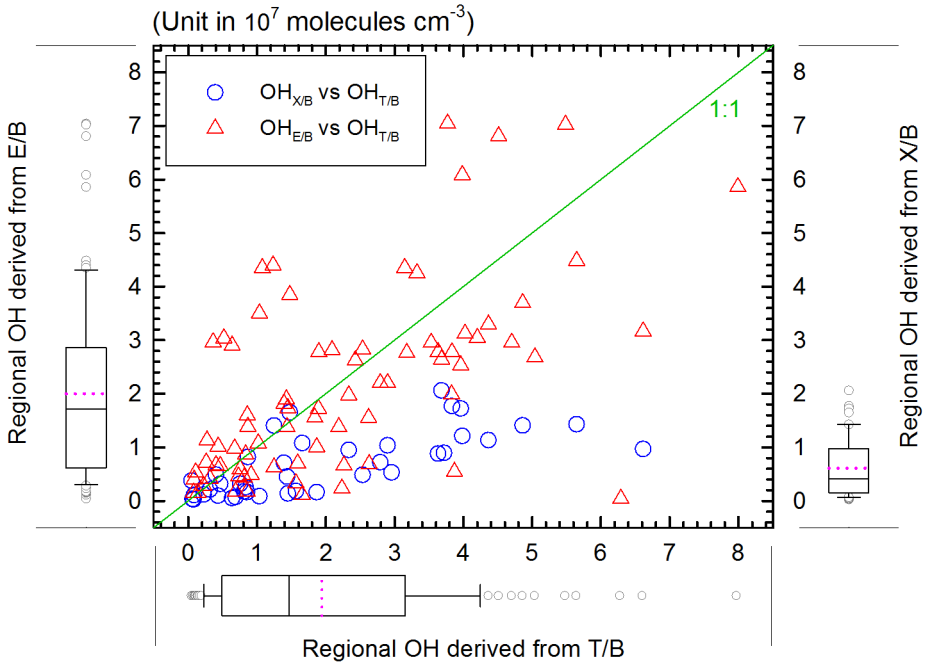

Fig. S8: Scatterplots of the regional mixing ratios of OH during 09:00 – 15:00 LST derived from the toluene/benzene ($OH_{T/B}$), ethylbenzene/benzene ($OH_{E/B}$) and m,p-xylene/benzene ($OH_{X/B}$) ratios. The green line denotes a 1:1 relationship. Next to axes are the box and whisker plots of each result, and the pink dotted lines denote the mean values.

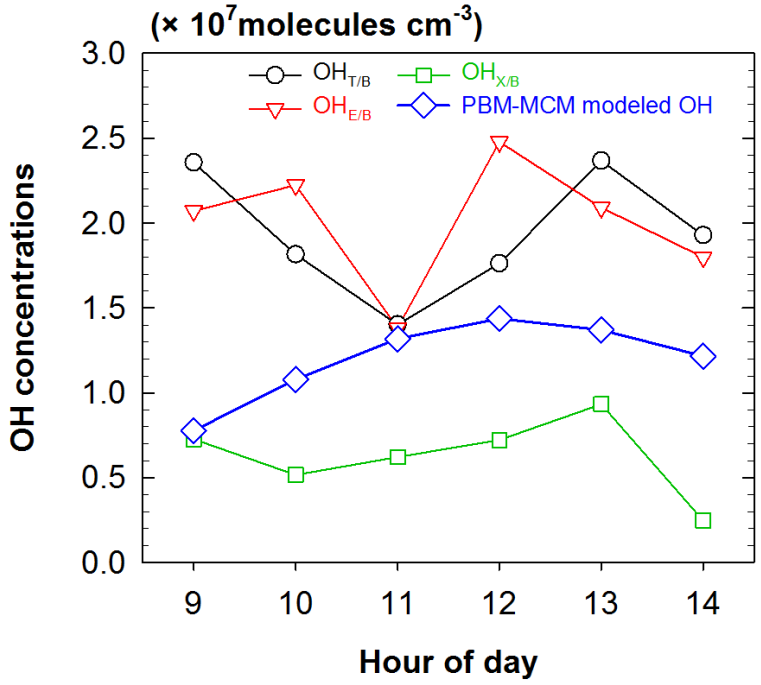

Fig. S9: Average hourly variations of the regional concentrations of OH derived from the toluene/benzene ratio ($OH_{T/B}$), ethylbenzene/benzene ratio ($OH_{E/B}$) and m,p-xylene/benzene ratio ($OH_{X/B}$) and the site-level OH modelled by PBM-MCM between 09:00 and 15:00 LST.

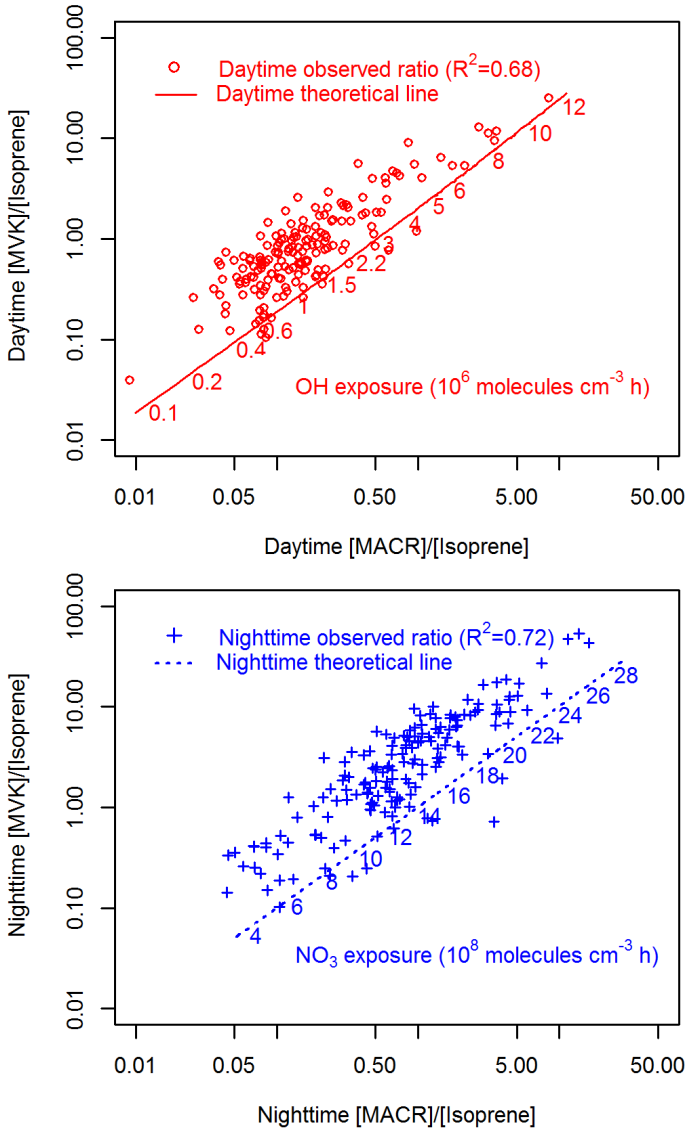

Fig. S10: Ranges of exposure derived by the progression of product/parent ratios (*i.e.* [MVK]/[isoprene] and [MACR]/[isoprene], unit: molecules cm^{-3} / molecules cm^{-3}). Red circles and blue crosses show the observed ratios for the daytime and nighttime measurements, respectively. The red solid and blue dashed lines are the theoretical product/parent ratios of isoprene sequential reaction scheme calculation. The numbers next to the line indicate the theoretical exposures (the product of radical concentration and reaction time) corresponding to any given product –parent relationship.

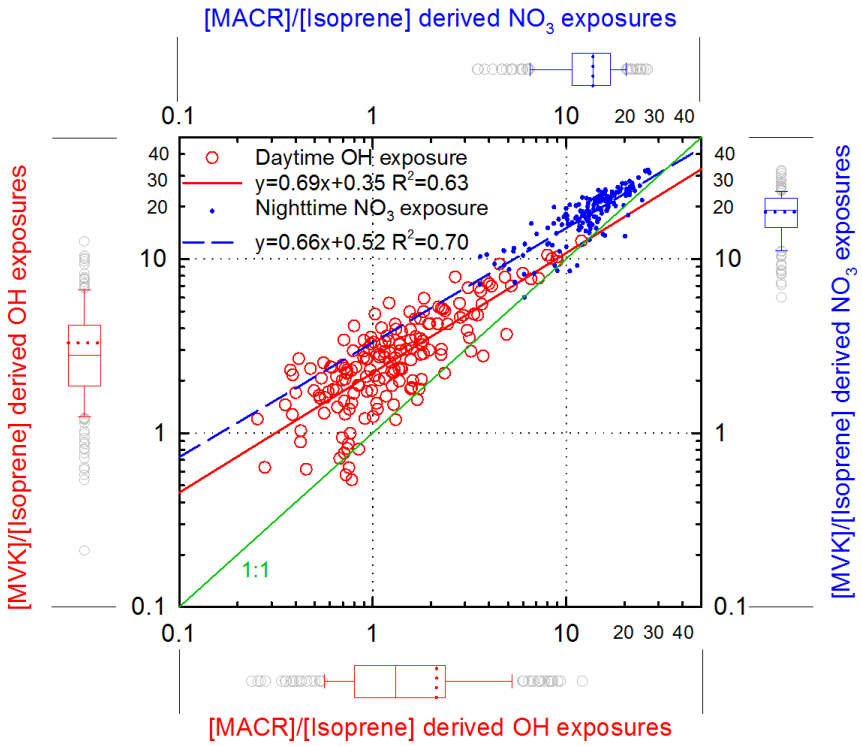

Fig. S11: Scatter plots of exposures derived from observed [MVK]/[isoprene] versus that from [MACR]/[isoprene]. The unit of OH exposure and NO_3 exposure is 10^6 molecules cm^{-3} h and 10^8 molecules cm^{-3} h, respectively.

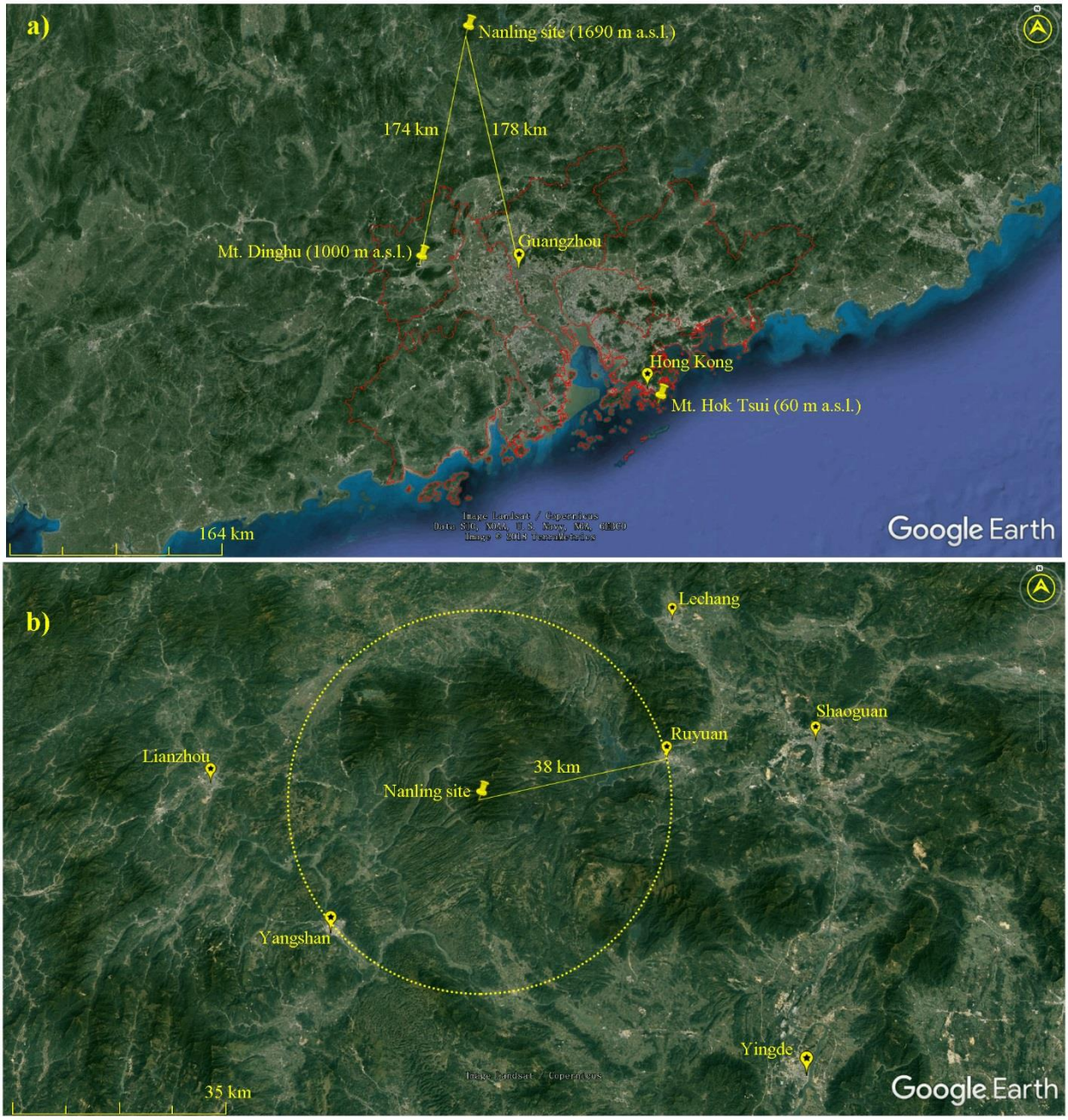

Fig. S12: (a) Location of the Nanling site, Dinghu Mountain site, Hok Tsui site, Guangzhou and Hong Kong. The Nanling site is 174 km northeast to the Dinghu Mountain site and 178 km northwest to Guangzhou. Red outlined domain represent the Pearl River Delta region. (b) Map showing the nearest urban centers (Yangshan County, Ruyuan County, Lechang City, Lianzhou City, Shaoguan City and Yingde City) around the site.

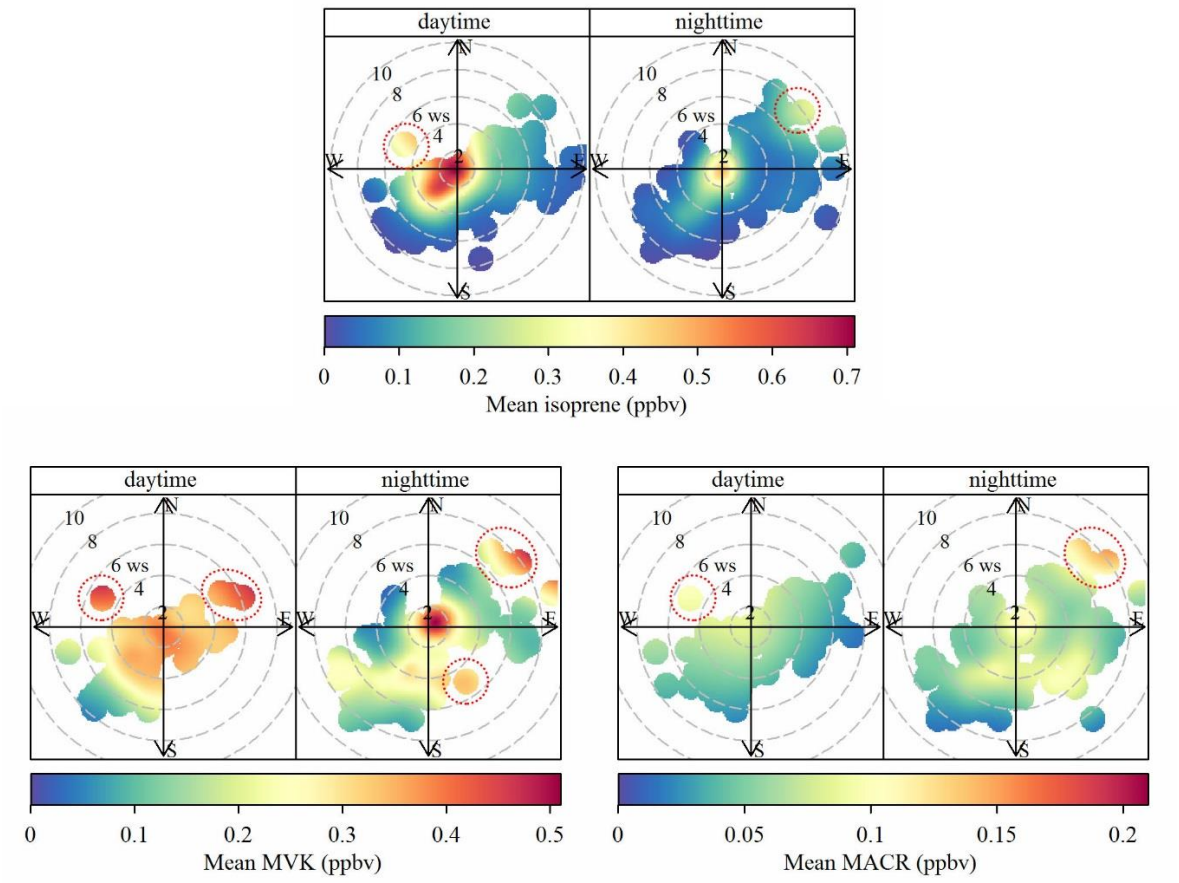

Fig. S13: Daytime and nighttime polarplots of isoprene, MVK and MACR during the sampling period (Jul 15–Aug 17 2016). Concentrations varied by wind speed (ws, unit in m/s) and wind direction. Red dotted sectorial domains represent the interferences of regional transport from nearby urban centres.